there may be some relationship between normal tension glaucoma and optic atrophy, and also emphasizes the importance of genetic changes that sensitize the retina and optic nerve to minor elevations of even normal intraocular pressure.

BIOCHEMISTRY AND PATHOLOGY OF POAG

Histological changes

It is estimated that roughly 20 to 50% of the large retinal ganglion cells (RGC) are lost in POAG. Although the reduction of RGC density occurs equally throughout the retina, visual sensitivity is first lost in areas where the initial RGC density is low, especially in the peripheral regions of the retina. As the disease progresses, atrophy of the nerve fiber layer is usually observed as additional RGC is lost. Typically, vertical collapse of the optic nerve head (ONH), loss of the neural rim at the ONH, rearrangement of central blood vessels, and loss of supporting tissue occur. Scanning electron microscopy of retinas with early stages of glaucoma shows evidence of initial collapse of the anterior lamina cribrosa, primarily in the vertical poles of the optic nerve head. Based on primate studies, optic cups with larger diameters are more susceptible to high ocular pressure and thus to glaucoma.

Role of the trabecular meshwork

Trabecular meshwork (TM) is a lamellated sheet of complex tissue that covers the inner wall of Schlemm's canal. TM has uniquely developed at the angle of primates, filtering the aqueous humor out of the eye. TM consists of two parts: the nonfiltering portion mainly occupied by trabecular cells and the filtering portion. Trabecular cells are highly phagocytic cells removing particles, cell debris, and protein from the aqueous humor. The first glaucoma locus, the *trabecular meshwork inducible glucocorticoid response* (TIGR), also known as myocilin, initially was identified by looking at genes whose transcription is highly induced by steroids in these cells. The filtering portion consists of three tissues: the cribriform layer, the corneoscleral meshwork, and the uveal meshwork. These trabecular beams or strands are intertwiningly connected to each other, forming a complex filtering mesh surrounding Schlemm's canal. The trabecular beams are thickened by accumulation of extracellular materials and decrease of cell density within the corneoscleral and uveal meshwork in aged eyes.

ANIMAL MODELS OF POAG

Overview: Difficulty of modeling the human eye

Limited access to appropriate biological materials, especially eye samples from affected donors at different stages of the POAG, is an impediment to the study of mechanisms underlying the disease. Because of the extreme difficulty in obtaining such diseased eyes from both patients and normal controls, animal models play a crucial role in investigating the biological pathway of disease development and in testing therapeutic strategies.

Different types of animal models for POAG have been found or created to mimic the optic nerve damage to resemble POAG phenotypes in humans. The greatest difficulty in constructing an animal model for POAG lies in the diversity of the anterior structures of the eye among different species (Tripathi and Tripathi, 1972, 1973). These structural differences include different iridocorneal angles or absence of specific quadrants from the TM. Nevertheless, within the limited areas in which interpretation of the data from a specific animal model parallels that in the human, various animals including the cow, dog, cat, horse, rabbit, chicken, and monkey can be used to observe POAG under various experimental conditions.

Animal models of POAG

Various animal models for inducible glaucoma have been reported. Argon laser photocoagulation of the TM in rhesus monkeys results in sustained elevation of IOP and has been used extensively to study early damage to the optic nerve head (May *et al.*, 1997). Corticosteroids such as betamethasone and dexamethasone have been used to treat rabbits, dogs, and cats to develop ocular hypertension (Bonomi *et al.*, 1978). Steroid treatment generally produces progressive glaucoma, but this process is reversed after about two months after cessation of the steroid. Trabecular blockage caused by inflammation after α-chymotrypsin treatment also has been used to produce elevated IOP in rabbit and monkey eyes (Vareilles *et al.*, 1977). Some types of avian species (chicken, quail, and turkey) have been known to develop elevated IOP as a consequence of continuous exposure to light.

Mouse models of glaucoma

Naturally occurring inherited animal glaucoma models are rare. However, extensive classification of IOP in mouse strains and molecular biological techniques to manipulate certain genes to produce transgenic or knockout/knockin mice recently have resulted in the development of a number of animal models with definitely known genetic causes for their disease (Chang *et al.*, 1999). As discussed earlier, four genes, myocilin (MYOC, TIGR), cytochrome P4501B1 (CYP1B1), optineurin (OPTN), and WDR36, currently are associated with glaucoma. OPTN, mutations of which are responsible for 16.7% of families with hereditary human NTG, is homologous to an inhibitory regulatory subunit of the high molecular kinase complex for the phosphorylation of NF-κB. Some of its known functions include inhibition of the tumor necrosis factor-alpha pathway, interaction with transcription factor IIIA, and mediation of the Huntington and Rab8 interaction for regulation of

membrane trafficking and cellular morphogenesis. OPTN is induced by TNF-α and binds to an inhibitor of TNF-α and the adenovirus E3-14.7 kDa protein. To determine the effects of human glaucoma mutations in a transgenic mouse system, mice over-expressing wild type OPTN, OPTN carrying the glaucoma associated mutation E50K, and OPTN with exon5 deleted were constructed. Although wild-type OPTN do not show any abnormalities and the exon 5 deleted construction was found to be lethal prenatally, mice transgenic for the E50K mutant OPTN show steep optic nerve cupping with rearrangement of supporting tissue and blood vessels 18 weeks after birth (see Figure 68.6). The RGC and astrocyte loss observed is similar to the end phase changes seen in human glaucoma patients. Understanding the mechanism underlying normal tension glaucoma in these transgenic mice will enhance our understanding of each step leading to optic nerve cupping and how to prevent it. Based on the success of the mouse model, use of larger animals such as transgenic rabbits or pigs, in which more precise measurement of IOP and trials of surgical procedures suitable for therapy in humans are possible are currently being investigated.

Other glaucoma mouse models have been made through genetic manipulation. Knockout and transgenic mouse models of myocilin were made to answer the question whether elevated expression of the myocilin protein can influence the IOP (Gould *et al.*, 2004). Up to a fifteen-fold increase in myocilin expression failed to result in elevation of the IOP, any abnormality of retinal ganglion cells, or cupping of the optic nerve head. Mice lacking the cytochrome P450 1B1 (CYP1B1) gene were generated on B6 and 129X1/SvJ mouse stains (Libby *et al.*, 2003). Both strains were affected by the CYP1B1 deficiency with focal angle abnormalities, but 129X1/SvJ albino strains lacking tyrosinase were more severely affected, suggesting the presence of tyrosinase as an important developmental molecule.

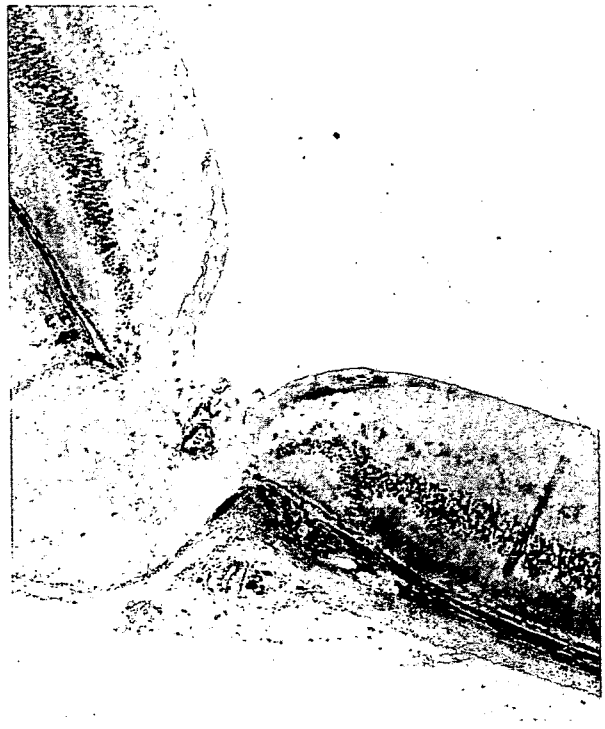

Figure 68.6 Histological section demonstrating excavation of the optic disc in an 18-week-old E50K mutant OPTN transgenic mouse.

Conclusion

In this chapter we have provided a brief overview of age-related eye diseases and the current state of knowledge and research on three of these. Age-related cataracts, age-related macular degeneration, and progressive open angle glaucoma account for much of the population burden imposed by age-related eye diseases. Although no perfect system to study these diseases exists today, an increasing number of experimental models are being developed. Although none is an exact replica of the clinical disease and should not be applied indiscriminately, each of these can provide useful information on some aspects of the disease in humans. They promise to accelerate the pace of research and provide mechanistic and therapeutic insights into the diseases that threaten sight in our aging population.

Recommended Resources

Albert, D.M. and Jakobiec, F.A. (Eds.) (2000). *Principles and Practice of Ophthalmology, 2e.* Philadelphia: W.B. Saunders Co.

Scriver, C.R. *et al.* (Eds.) (2005). *The Metabolic and Molecular Bases of Inherited Disease*, 8e. New York: McGraw-Hill.

Tasman, W. and Jaeger, E. (Eds.) (2001). *Duane's Clinical Ophthalmology*. Philadelphia: J.B. Lippincott Co.

REFERENCES

Ali, R.R., Sarra, G.M., Stephens, C., Alwis, M.D., Bainbridge, J.W., Munro, P.M. *et al.* (2000). Restoration of photoreceptor ultrastructure and function in retinal degeneration slow mice by gene therapy. *Nat. Genet. 25 (3)*, 306–310.

Ambati, J., Anand, A., Fernandez, S., Sakurai, E., Lynn, B.C., Kuziel, W.A. *et al.* (2003). An animal model of age-related macular degeneration in senescent Ccl-2- or Ccr-2-deficient mice. *Nat. Med. 9 (11)*, 1390–1397.

Anderson, D.H., Mullins, R.F., Hageman, G.S., and Johnson, L.V. (2002). A role for local inflammation in the

formation of drusen in the aging eye. *Am. J. Ophthalmol. 134 (3)*, 411–431.

Bonomi, L., Perfetti, S., Noya, E., Bellucci, R., and Tomazzoli, L. (1978). Experimental corticosteroid ocular hypertension in the rabbit. *Albrecht. Von. Graefes Arch. Klin. Exp. Ophthalmol. 209 (2)*, 73–82.

Brady, J.P., Garland, D., Duglas-Tabor, Y., Robison, W.G. Jr., Groome, A., and Wawrousek, E.F. (1997). Targeted disruption of the mouse alpha A-crystallin gene induces cataract and cytoplasmic inclusion bodies containing the small heat shock protein alpha B-crystallin. *Proc. Natl. Acad. Sci. USA 94*, 884–889.

Buch, H., Vinding, T., La Cour, M., Appleyard, M., Jensen, G.B., and Nielsen, N.V. (2004). Prevalence and causes of visual impairment and blindness among 9980 Scandinavian adults: The Copenhagen City Eye Study. *Ophthalmology 111 (1)*, 53–61.

Chader, G.J. (2002). Animal models in research on retinal degenerations: Past progress and future hope. *Vision Res. 42 (4)*, 393–399.

Chang, B., Smith, R.S., Hawes, N.L., Anderson, M.G., Zabaleta, A., Savinova, O. *et al.* (1999). Interacting loci cause severe iris atrophy and glaucoma in DBA/2J mice. *Nat. Genet. 21 (4)*, 405–409.

Congdon, N.G., Friedman, D.S., and Lietman, T. (2003). Important causes of visual impairment in the world today. *J.A.M.A. 290 (15)*, 2057–2060.

Crabb, J.W., Miyagi, M., Gu, X., Shadrach, K., West, K.A., Sakaguchi, H. *et al.* (2002). Drusen proteome analysis: An approach to the etiology of age-related macular degeneration. *Proc. Natl. Acad. Sci. USA 99 (23)*, 14682–14687.

Davies, M.J. and Truscott, R.J. (2001). Photo-oxidation of proteins and its role in cataractogenesis. *J. Photochem. Photobiol. B 63 (1–3)*, 114–125.

Edwards, A.O., Ritter, R. III, Abel, K.J., Manning, A., Panhuysen, C., and Farrer, L.A. (2005). Complement factor H polymorphism and age-related macular degeneration. *Science 308 (5720)*, 421–424.

Giblin, F.J., Padgaonkar, V.A., Leverenz, V.R., Lin, L.R., Lou, M.F., Unakar, N.J. *et al.* (1995). Nuclear light scattering, disulfide formation and membrane damage in lenses of older guinea pigs treated with hyperbaric oxygen. *Exp. Eye Res. 60 (3)*, 219–235.

Gould, D.B., Miceli-Libby, L., Savinova, O.V., Torrado, M., Tomarev, S.I., Smith, R.S. *et al.* (2004). Genetically increasing Myoc expression supports a necessary pathologic role of abnormal proteins in glaucoma. *Mol. Cell Biol. 24 (20)*, 9019–9025.

Graw, J. and Loster, J. (2003). Developmental genetics in ophthalmology. *Ophthalmic Genet. 24 (1)*, 1–33.

Hammond, C.J., Webster, A.R., Snieder, H., Bird, A.C., Gilbert, C.E., and Spector, T.D. (2002). Genetic influence on early age-related maculopathy: A twin study. *Ophthalmology 109 (4)*, 730–736.

Hanson, S.R., Hasan, A., Smith, D.L., and Smith, J.B. (2000). The major in vivo modifications of the human water-insoluble lens crystallins are disulfide bonds, deamidation, methionine oxidation and backbone cleavage. *Exp. Eye Res. 71 (2)*, 195–207.

Heiba, I.M., Elston, R.C., Klein, B.E., and Klein, R. (1994). Sibling correlations and segregation analysis of age-related maculopathy: The Beaver Dam Eye Study. *Genet. Epidemiol. 11 (1)*, 51–67.

Hejtmancik, J.F., Kaiser-Kupfer, M.I., and Piatigorsky, J. (2001). Molecular biology and inherited disorders of the eye lens. In C.R. Scriver *et al.* (Eds.). *The Metabolic and Molecular Basis of Inherited Disease, 8e.* New York: McGraw Hill.

Hejtmancik, J.F. and Kantorow, M. (2004). Molecular genetics of age-related cataract. *Exp. Eye Res. 79 (1)*, 3–9.

Hejtmancik, J.F. and Smaoui, N. (2003). Molecular Genetics of Cataract. In B. Wissinger, S. Kohl, and U. Langenbeck (Eds.). *Genetics in Ophthalmology.* Basel: S. Karger.

Klein, B.E., Klein, R., Sponsel, W.E., Franke, T., Cantor, L.B., Martone, J. *et al.* (1992). Prevalence of glaucoma. The Beaver Dam Eye Study. *Ophthalmology 99 (10)*, 1499–1504.

Kuck, J.F. (1990). Late onset hereditary cataract of the Emory mouse. A model for human senile cataract. *Exp. Eye Res. 50*, 659–664.

Libby, R.T., Smith, R.S., Savinova, O.V., Zabaleta, A., Martin, J.E., Gonzalez, F.J. *et al.* (2003). Modification of ocular defects in mouse developmental glaucoma models by tyrosinase. *Science 299 (5612)*, 1578–1581.

May, C.A., Hayreh, S.S., Furuyoshi, N., Ossoinig, K., Kaufman, P.L., and Lutjen-Drecoll, E. (1997). Choroidal ganglion cell plexus and retinal vasculature in monkeys with laser-induced glaucoma. *Ophthalmologica 211 (3)*, 161–171.

McCarty, C.A. and Taylor, H.R. (2001). The genetics of cataract. *Invest Ophthalmol. Vis. Sci. 42 (8)*, 1677–1678.

Mullins, R.F., Russell, S.R., Anderson, D.H., and Hageman, G.S. (2000). Drusen associated with aging and age-related macular degeneration contain proteins common to extracellular deposits associated with atherosclerosis, elastosis, amyloidosis, and dense deposit disease. *FASEB J. 14 (7)*, 835–846.

Okano, Y., Asada, M., Fujimoto, A., Ohtake, A., Murayama, K., Hsiao, K.J. *et al.* (2001). A genetic factor for age-related cataract: identification and characterization of a novel galactokinase variant, "Osaka," in Asians. *Am. J. Hum. Genet. 68 (4)*, 1036–1042.

Roth, F., Bindewald, A., and Holz, F.G. (2004). Key pathophysiologic pathways in age-related macular disease. *Graefes Arch. Clin. Exp. Ophthalmol. 242 (8)*, 710–716.

Seddon, J.M., Ajani, U.A., and Mitchell, B.D. (1997). Familial aggregation of age-related maculopathy. *Am. J. Ophthalmol. 123 (2)*, 199–206.

Spector, A. (1995). Oxidative stress-induced cataract: mechanism of action. *FASEB J. 9 (12)*, 1173–1182.

Stafford, T.J., Anness, S.H., and Fine, B.S. (1984). Spontaneous degenerative maculopathy in the monkey. *Ophthalmology 91 (5)*, 513–521.

The Italian-American Cataract Study Group (1991). Risk factors for age-related cortical, nuclear, and posterior subcapsular cataracts. *Am. J. Epidemiol. 133*, 541–553.

Thylefors, B., Negrel, A.D., Pararajasegaram, R., and Dadzie, K.Y. (1995). Global data on blindness. *Bull. World Health Organ 73 (1)*, 115–121.

Tripathi, R.C. and Tripathi, B.J. (1972). The mechanism of aqueous outflow in lower mammals. *Exp. Eye Res. 14 (1)*, 73–79.

Tripathi, R.C. and Tripathi, B.J. (1973). The mechanism of aqueous outflow in birds. I. An ultrastructural study of normal eyes. *Exp. Eye Res. 15 (3)*, 409–423.

Tuo, J., Bojanowski, C.M., and Chan, C.C. (2004). Genetic factors of age-related macular degeneration. *Prog. Retin. Eye Res. 23 (2)*, 229–249.

Umeda, S., Ayyagari, R., Okamoto, H., Suzuki, M.T., Terao, K., Mizota, A. *et al.* (2005). Linkage and mutation analysis to identify the gene associated with macular degeneration segregating in a cynomolgus monkey. *Invest. Ophthalmol. Vis. Sci. 46*, 683–691.

Vareilles, P., Silverstone, D., Plazonnet, B., Le Douarec, J.C., Sears, M.L., and Stone, C.A. (1977). Comparison of the effects of timolol and other adrenergic agents on intraocular pressure in the rabbit. *Invest. Ophthalmol. Vis. Sci. 16 (11)*, 987–996.

Proteomic and Transcriptomic Analyses of Retinal Pigment Epithelial Cells Exposed to REF-1/TFPI-2

Masahiko Shibuya,[1,2] *Haru Okamoto,*[1] *Takehiro Nozawa,*[3] *Jun Utsumi,*[4] *Venkat N. Reddy,*[5] *Hirotoshi Echizen,*[2] *Yasuhiko Tanaka,*[6] *and Takeshi Iwata*[1]

Purpose. The authors previously reported a growth-promoting factor, REF-1/TFPI-2, that is specific to retinal pigment epithelial (RPE) cells. The purpose of this study was to determine the genes and proteins of human RPE cells that are altered by exposure to TFPI-2.

Methods. Human primary RPE cells were cultured with or without TFPI-2. Cell extracts and isolated RNA were subjected to proteomic and transcriptomic analyses, respectively. Proteins were separated by two-dimensional gel electrophoresis followed by gel staining and ion spray tandem mass spectrometry analyses. Transcriptomic analysis was performed using a DNA microarray to detect 27,868 gene expressions.

Results. Proteomic analysis revealed c-Myc binding proteins and ribosomal proteins L11 preferentially induced by TFPI-2 in human RPE cells. Transcriptomic analysis detected 10,773 of 33,096 probes in the TFPI-2 treated samples, whereas only 2186 probes were detected in the nontreated samples. Among the genes up-regulated by TFPI-2 at the protein level were *c-myc*, Mdm2, transcription factor E2F3, retinoblastoma binding protein, and the *p21* gene, which is associated with the *c-myc* binding protein and ribosomal protein L11.

Conclusions. The mechanisms by which TFPI-2 promotes the proliferation of RPE cells may be associated with augmented *c-myc* synthesis and the activation of E2F in the retinoblastoma protein (Rb)/E2F pathway at the G1 phase of the RPE cells. Activation of ribosomal protein L11 and the Mdm2 complex of the p53 pathway may be counterbalanced by the hyperproliferative conditions. (*Invest Ophthalmol Vis Sci.* 2007;48: 516-521) DOI:10.1167/iovs.06-0434

Retinal pigment epithelial (RPE) cells play important roles in maintaining the homeostasis of the retina. RPE cells, located between the sensory retina and the choroidal blood supply, form a diffusion barrier controlling access to the subretinal space, with the RPE membrane regulating the transport of proteins and controlling the hydration and ionic composition of the subretinal space. The sensitivity and viability of the photoreceptors thus depend on RPE-catalyzed transport activity. Proteins in the RPE cells that function in ionic, sugar, peptide, and water transport have been identified.[1] Damage to RPE cells generally leads to degeneration of the neural retina, as occurs in retinitis pigmentosa and age-related macular degeneration. Transplantation of the healthy retinal pigment cells or embryonic stem cells differentiating into RPE cells would be an ideal therapeutic approach to treat such diseases, and such attempts have been made.[2]

An alternative approach to treat these retinal diseases would be the use of a growth factor that promotes proliferation of the remaining RPE cells in a damaged retina or one that stimulates the regeneration of damaged RPE cells. To find such factor(s), the proteins expressed in human fibroblast cells were fractionated and assayed, leading to the isolation of RPE cell factor-1 (REF-1), which selectively promoted the proliferation of primary human RPE cells.[3]

Subsequently, the cDNA of REF-1 was cloned using information from the N-terminal amino acid sequences, which was identical with the tissue factor pathway inhibitor-2 (TFPI-2).[3] Earlier studies have shown that TFPI-2 is a Kunitz-type serine protease inhibitor[4-6] involved in the regulation of extrinsic blood coagulation[4,7] and in the proliferation, invasion, and metastasis of various types of malignant cells.[4,8-13] Extensive studies on the physiological roles of TEPI-2 have revealed that the ERK/MAPK pathway[13] may be associated with the up-regulation of the *TFPI-2* gene and that DNA methylation[9,10] in certain tumor cell lines may be related to the downregulation of the *TEPI-2* gene. When TFPI-2 is added to the culture medium of vascular smooth muscle cells, it promotes cell proliferation.[14]

Our initial finding that TFPI-2 enhanced RPE proliferation prompted us to question how this was achieved. We applied proteomic and transcriptomic analyses to screen the changes in the expression of the RNAs and proteins in RPE cells and will show that the proliferation promoting activity of TFPI-2 on RPE cells is associated with the regulation of an oncogene product, *c-myc*, and representative cancer repressor proteins retinoblastoma protein (Rb)/E2F and p53.

Materials and Methods

TFPI-2 Treatment of Human RPE Cell Culture

Human primary RPE cells (passage 5) were seeded at a density of 2.5×10^4 cells/0.5 mL per well in 24-well plastic plates (BD Biosciences, Franklin Lakes, NJ) with Dulbecco modified MEM (DMEM; Invitrogen Japan, Tokyo, Japan) containing 15% fetal calf serum (FCS, Invitrogen). TFPI-2 was added to 20 wells with the RPE cells at 10 ng/mL concentrations and was incubated at 37°C for 24 hours for the proteomic samples, and for 6 hours, 12 hours, and 24 hours for the transcriptomic samples. An equal amount of saline was added to 20 wells containing RPE cells for controls. TFPI-2 was donated by Toray Industries, Inc., Tokyo, Japan.

From the [1]Laboratory of Cellular and Molecular Biology, National Institute of Sensory Organs, National Hospital Organization Tokyo Medical Center, Tokyo, Japan; [2]Department of Pharmacotherapy, Meiji Pharmaceutical University, Tokyo, Japan; [3]Analytical Instrument Division, AMR Inc., Tokyo, Japan; [4]R&D Division, Toray Industries, Inc., Tokyo, Japan; [5]Department of Ophthalmology, Kellogg Eye Center, University of Michigan, Ann Arbor, Michigan; and [6]International University of Health and Welfare, Mita Hospital, Tokyo, Japan.

Supported in part by a grant-in-aid from the policy-based Medical Services Foundation.

Submitted for publication April 18, 2006; revised July 17, 2006; accepted December 4, 2006.

Disclosure: **M. Shibuya**, None; **H. Okamoto**, None; **T. Nozawa**, AMR Inc. (F); **J. Utsumi**, Toray Industries, Inc. (F); **V.N. Reddy**, None; **H. Echizen**, None; **Y. Tanaka**, None; **T. Iwata**, None

The publication costs of this article were defrayed in part by page charge payment. This article must therefore be marked "*advertisement*" in accordance with 18 U.S.C. §1734 solely to indicate this fact.

Corresponding author: Takeshi Iwata, Laboratory of Cellular and Molecular Biology, National Institute of Sensory Organs, National Hospital Organization Tokyo Medical Center, 2-5-1 Higashigaoka, Meguro-ku, Tokyo 152-8902, Japan; iwatatakeshi@kankakuki.go.jp.

Investigative Ophthalmology & Visual Science, February 2007, Vol. 48, No. 2

Protein Sample Preparation

To isolate whole cellular protein extracts from cultured RPE cells, the cells were rinsed 3 times with 1× PBS (pH 7.4) and were lysed in a denaturing lysis buffer containing 7 M urea, 2 M thiourea, 4% CHAPS, 40 mM Tris, 0.2% purifier (Bio-Lyte, pH range 3–10; Bio-Rad, Hercules, CA), and 50 mM dithiothreitol (DTT). The collected lysate was then centrifuged at 14,000*g* for 15 minutes at 4°C. Proteins in the supernatant were repeatedly concentrated and precipitated and finally desalinated (Readyprep 2-D Cleanup kit; Bio-Rad). The protein concentration in the RPE samples was determined by a modified Lowry method adapted for use with the lysis buffer.

Two-Dimensional Electrophoresis

Protein samples were separated by a two-dimensional electrophoresis method. A 300-μg protein sample was loaded on immobilized pH gradient (IPG) strips (pH 3–10, 7 cm; pH 4–7, 17 cm; Bio-Rad) by in-gel rehydration at 20°C overnight. For the 7-cm strip, isoelectric focusing (IEF) was used for the first dimension at an initial voltage of 250 V for 15 minutes, increased to 4000 V for 2 hours, and held until 20,000 V/h was reached. For the 17-cm strip, the initial voltage was set at 250 V, as for the 7-cm strip. Then the voltage was increased to 10,000 V for 3 hours and was held until 60,000 V/h was reached. Immediately after IEF, the IPG strips were equilibrated for 20 minutes in buffer containing 6 M urea, 2% SDS, 0.375 M Tris (pH 8.8), and 20% glycerol under a reduced condition with 2% DTT (Bio-Rad), followed by another incubation for 10 minutes in the same buffer under alkylating conditions with 2.5% iodoacetamide (Bio-Rad).[15]

Equilibrated IPG strips were then electophoresed by SDS-PAGE for the second dimension. Images of the chemiluminescent signals were captured and merged with those of protein spots made visible by protein gel stain (Sypro Ruby; Bio-Rad), and the spots corresponding to the immunoreactivity were cut out. To test reproducibility, the experiment was performed twice.

Protein Identification by Mass Spectrometry

Excised gel pieces were rinsed with water and then with acetonitrile and were completely dried for the reduction-alkylation step. They were incubated with 10 mM DTT in 100 mM ammonium bicarbonate for 45 minutes at 56°C, then with 55 mM iodoacetamide in 100 mM ammonium bicarbonate for 30 minutes at room temperature in the dark. The supernatant was removed, and the washing procedure was repeated three times. Finally, the gel pieces were again completely dried before trypsin digestion and were rehydrated in a solution of trypsin (12.5 ng/μL; Promega, Madison, WI) in 50 mM ammonium bicarbonate. The digestion was continued for 16 hours at 37°C, and the extraction step was performed once with 25 mM ammonium bicarbonate, then twice with 5% formic acid, and finally with water. After resuspension in 40 μL solution of aqueous 0.1% trifluoroacetic acid/2% acetonitrile, the samples were analyzed by liquid chromatography coupled to tandem mass spectrometry (LC-MS/MS). For analysis by LC-MS/MS, the tryptic digests were injected by an automatic sampler (HTS-PAL, CTC Analytics, Zwingen, Switzerland) onto a 0.2 × 50-mm capillary reversed-phase column (Magic C18, 3 μm; Michrom BioResources, Inc., Auburn, CA) using an HPLC (Paradigm MS4; Michrom BioResources). Peptides were eluted with a gradient (95% solvent A consisting of 98% H_2O/2% acetonitrile/0.1% formic acid)/5% solvent B (10% H_2O/90% acetonitrile/0.1% formic acid; 0 minute)/35% solvent A/65% solvent B (20 minutes)/5% solvent A/95% solvent B (21 minutes)/5% solvent A/95% solvent B (23 minutes)/95% solvent A/5% solvent B (30 minutes) for 30 minutes at a flow rate of 1.5 μL/min. Peptides were eluted directly into an ion trap mass spectrometer (ESI; Finnigan LTQ; Thermo Electron Corporation, Waltham, MA) capable of data-dependent acquisition. Each full MS scan was followed by an MS/MS scan of the most intense peak in the full MS spectrum with the dynamic exclusion enabled to allow detection of less-abundant peptide ions. Mass spectrometric scan events and HPLC solvent gradients were controlled with the use of a computer program (Paradigm Home; Michrom BioResources).

Total RNA Isolation from RPE Cells

Total RNA was isolated from the cultured RPE cells after 6 hours, 12 hours, and 24 hours with TFPI-2 using a total RNA isolation kit (RNA-Bee-RNA Isolation Reagent; Tel-Test, Friendswood, TX). Total RNA samples were treated with RNase-free DNase (Roche Diagnostics Japan) to minimize genomic DNA contamination.

DNA Microarray Analysis

DNA microarray analysis was performed (AB1700 Chemiluminescent Microarray Analyzer; Applied Biosystems, Foster City, CA). The survey array used (Human Genome Survey Array; Applied Biosystems) contained 33,096 60-mer oligonucleotide probes representing a set of 27,868 individual human genes and more than 1000 control probes. Sequences used for the microarray probe were obtained from curated transcripts (Celera Genomics Human Genome Database), RefSeq transcripts that had been structurally curated from the LocusLink public database, high-quality cDNA sequences from the Mammalian Gene Collection (MGC; http://mgc.nci.nih.gov), and transcripts that were experimentally validated (Applied Biosystems). The 60-mer oligo probes were synthesized using standard phosphoramidite chemistry and solid-phase synthesis and underwent quality control by mass spectrometry. The probes were deposited and covalently bound to a derivatized nylon substrate (2.5 × 3 inches) that was backed by a glass slide by contact spotting with a feature diameter of 180 μm and more than 45 μm between each feature. A 24-mer oligo internal control probe (ICP) was cospotted at every feature with 60-mer gene expression probe on the microarray. Digoxigenin-UTP labeled cRNA was generated and linearly amplified from 1 μg total RNA (Chemiluminescent RT-IVT Labeling Kit, version 2.0; Applied Biosystems) according to the manufacturer's protocol. Array hybridization (two arrays per sample), chemiluminescence detection, image acquisition, and analysis were performed (Chemiluminescence Detection Kit and AB1700 Chemiluminescent Microarray Analyzer; Applied Biosystems) according to the manufacturer's protocol.

Briefly, each microarray was first prehybridized at 55°C for 1 hour in hybridization buffer with blocking reagent. Sixteen micrograms labeled cRNA targets were first fragmented into 100 to 400 bases by incubation with fragmentation buffer at 60°C for 30 minutes, mixed with internal control target (ICT; 24-mer oligo labeled with LIZR fluorescent dye), and hybridized to each prehybrid microarray in 1.5 mL vol at 55°C for 16 hours. After hybridization, the arrays were washed with hybridization wash buffer and chemiluminescence rinse buffer. Enhanced chemiluminescent signals were generated by first incubating the arrays with anti-digoxigenin alkaline phosphatase and enhanced with chemiluminescence enhancing solution and chemiluminescence substrate.

Images were collected from each microarray using the 1700 analyzer equipped with a high-resolution, large-format CCD camera, including 2 "short" chemiluminescent images (5-second exposure length each) and 2 "long" chemiluminescent images (25-second exposure length each) for gene expression analysis, two fluorescent images for feature finding and spot normalization, and two quality control images for spectrum cross-talk correction. Images were quantified, corrected for background and spot, and spatially normalized.

Data Analysis

MS data were identified with the use of a protein search program (BioWorks 3.2; Thermo Electron Corporation, Waltham, MA). For protein database searches, the same program was used to create centroid peak lists from the raw spectra. These peak lists were then submitted for database searching (BioWorks). The identity of the samples was searched from databases (nrNCBI [www.ncbi.nlm.nih.gov]) that extracted proteins and were restructured; search terms included human and *Homo saptens*. Differentially expressed proteins were further analyzed for related genes and proteins using natural language processing software (Pubgene database; PubGene Inc., Boston, MA) and data mining software of gene expression (OmniViz; OmniViz, Inc., Maynard, MA).

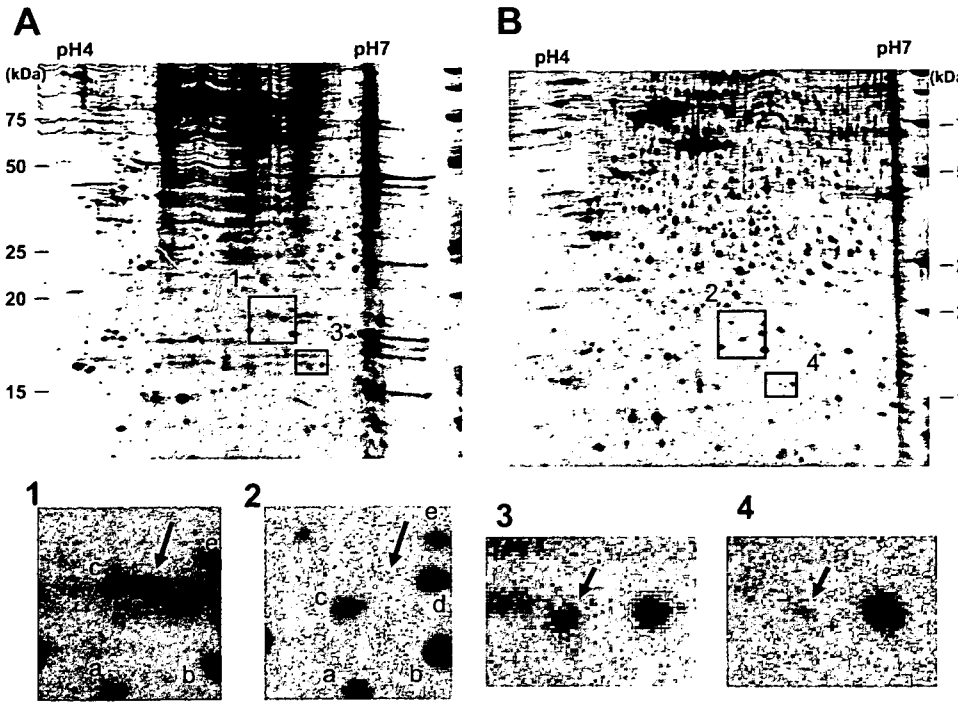

FIGURE 1. Two-dimensional gel electrophoresis of human RPE cells culture with (A) and without (B) TFPI-2. Spots corresponding to proteins whose expression is dependent on the presence of TFPI-2 in the culture medium are indicated by the *arrows* (*insets*). Proteins were detected by SYPRO Ruby staining. Spots corresponding to the differentially expressed proteins indicated by *arrows* (1 vs. 2 and 3 vs. 4) were subsequently subject to the LC-MS/MS analysis so that proteins could be identified.

RESULTS

Proteome Analysis of RPE Cells Treated with TFPI-2

To determine the mechanisms responsible for the proliferation-promoting activity of TFPI-2 on RPE cells, protein synthesis and RNA expression were determined before and after TFPI-2 exposure. Differentially expressed proteins in the primary human RPE cells in response to TFPI-2 were identified by two-dimensional electrophoresis (Fig. 1). Samples were initially separated using IPG at a pH range of 3 to 10 to observe the full distribution of protein spots. The pH range was then narrowed to 4 to 7 to obtain higher resolution for spot picking. Consequently, approximately 480 spots were identified in the whole gel. We then focused on molecular weight less than 25 kDa, which is easy to check for changes. Ten spots considered differentially expressed in the two-dimensional gel were collected and subjected to LC-MS/MS analysis. Among the identified proteins, ribosomal protein L11 (RPL11; Fig. 1-1) and c-Myc binding protein (MYCBP; Fig. 1-3), known for regulating cell proliferation, were identified.[16] These two proteins, identified by LC-MS/MS analysis and data analysis software (Bioworks 3.2), were consistent with those estimated from the results of two-dimensional electrophoresis (Table 1).

Transcriptomic Analysis of RPE Cells Treated with TFPI-2

The expression of 8134 genes in RPE cells was analyzed using DNA microarray with and without TFPI-2 exposure for 6 hours, 12 hours, and 24 hours. Signal normalization was performed for six independent DNA microarray chips according to the manufacturer's protocol. Genes differentially expressed by more than threefold were considered significant and were selected for further analysis. Among the 33,096 possible probes, 10,773 probes were detected in the RPE cells incubated with TFPI-2, whereas only 2186 probes were detected without TFPI-2. Based on expression levels at the three time points (6 hours, 12 hours, and 24 hours), the time-dependent expression pattern of each gene was calculated and clustered with other genes with similar expression patterns using data mining software (OmniViz). Data analysis resulted in 38 clusters of genes that either increased or decreased their expression levels by more than twofold after TFPI-2 (Fig. 2). Nineteen genes were upregulated in 5 clusters, 108 genes in 16 clusters, and 717 genes in 22 clusters at 6 hours, 12 hours, and 24 hours, respectively. For downregulated genes, 30 genes in 16 clusters, 119 genes in 19 clusters, and 3 genes in 19 clusters were observed after 6 hours, 12 hours, and 24 hours, respectively. Transcriptomic analysis revealed significantly more genes differentially expressed at the transcriptional level than at the proteome level.

DISCUSSION

Proteins and genes whose expression was upregulated or downregulated after exposure to TFPI-2 were analyzed in human RPE cells to study the proteomic and transcriptomic changes. Protein and gene expression profiles for human RPE cells have been reported by West et al.,[17] who identified 278 proteins, and Cai et al.,[18] who reported 5580 ± 84 genes expressed in adult human RPE and ARPE19 cell lines using a DNA chip with 12,600 probes (Human U95Av2; Affymetrix, Santa Clara, CA). Our study showed changes in the expression of 8134 of 27,868 genes. DNA microarray analyses were simul-

TABLE 1. Two-Dimensional Gel Spots Identified by Mass Spectrometry

Protein	Number of AA	Peptide Residues	Identified Peptide from Database	MW	Score	Accession Number
c-Myc binding protein	167	108–117	TAEDAKDFFK	18642.6	10.13	1731809
Ribosomal protein L11	177	88–94	VREYELR	20125.1	20.21	14719845

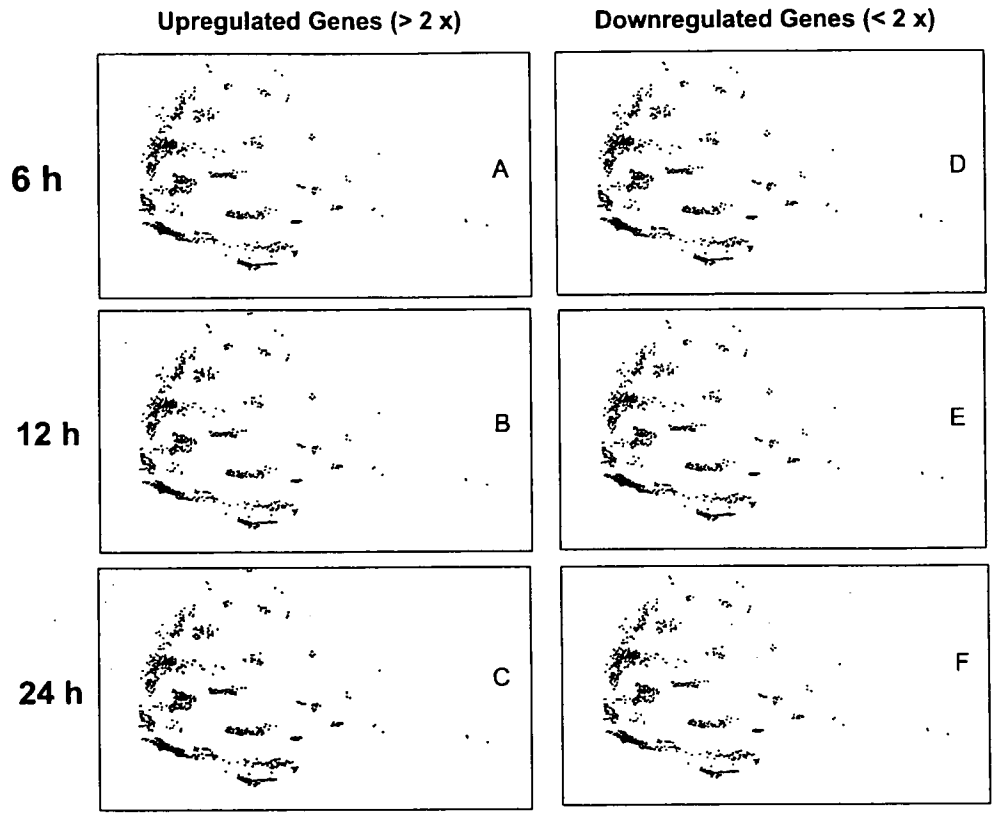

FIGURE 2. Differentially expressed genes detected by DNA array are plotted as clusters. Differentially expressed genes whose expression level was increased by more than twofold (A–C) or was reduced by more than 0.5-fold (D–F) in RPE cells treated with TFPI-2 at incubation times of 6 hours, 12 hours, and 24 hours compared with the control cells are shown. Expression profile analysis revealed different gene expression patterns at each incubation time.

taneously performed at three time points (6 hours, 12 hours, and 24 hours) to monitor the course of expression of the possible 27,868 genes in human RPE cells exposed and not exposed to TFPI-2. This study was conducted at the translational and the transcriptional levels to complement the disadvantages of each method.

Raw gene expression data were further analyzed with data mining software (OmniViz) to obtain an overall picture of the transcriptional changes induced by TFPI-2 in human primary RPE cells. Genes whose expressions were changed by more than twofold were clustered into 38 groups showing a change of expression at each time point (Fig. 2). The number of genes upregulated at each time point was considerably higher than the number that was downregulated. A small number of genes was triggered by TFPI-2 treatment at 6 hours, before the major changes occurred at 24 hours. Among the initially upregulated genes were reticulon 4 interacting protein 1, phospholipase C, delta 1, granzyme M (lymphocyte met-ase 1; *GZMM*), and mitochondrial ribosomal protein L41 (*MRPL41*).

Proteomics analysis simultaneously performed at 24 hours identified two differentially expressed proteins, the c-*myc* binding protein (MYCBP) and the ribosomal protein L11 (RPL11). MYCBP and RPL11 (Fig. 3) are well known to regulate cell cycling through the Rb/E2F pathway and the p53 pathway, respectively. MYCBP stimulates c-*myc* transcription through the retinoblastoma protein (Rb)/E2F pathway (see Fig. 5). Sears et al.[19] reported that activation of Myc increased the signal transduction of the cyclin D/cdk4 and cyclin E/cdk2 pathways. Activation of these pathways inactivates Rb after phosphorylation and E2F dissociation, which then promotes RPE cells to go into the S-phase of the cell cycle. The twofold transcriptional increase of *Rb* and *E2F3* in TFPI-2 exposed cells compared with control at 24 hours supports this hypothesis (Figs. 4C, 4F).

Concomitantly, the expressions of Rb and Mdm2 were upregulated twofold in growth-stimulated cells compared with control cells. Because Rb is associated with the negative regulation of the G_1-phase of the cell cycle, the enhanced expres-

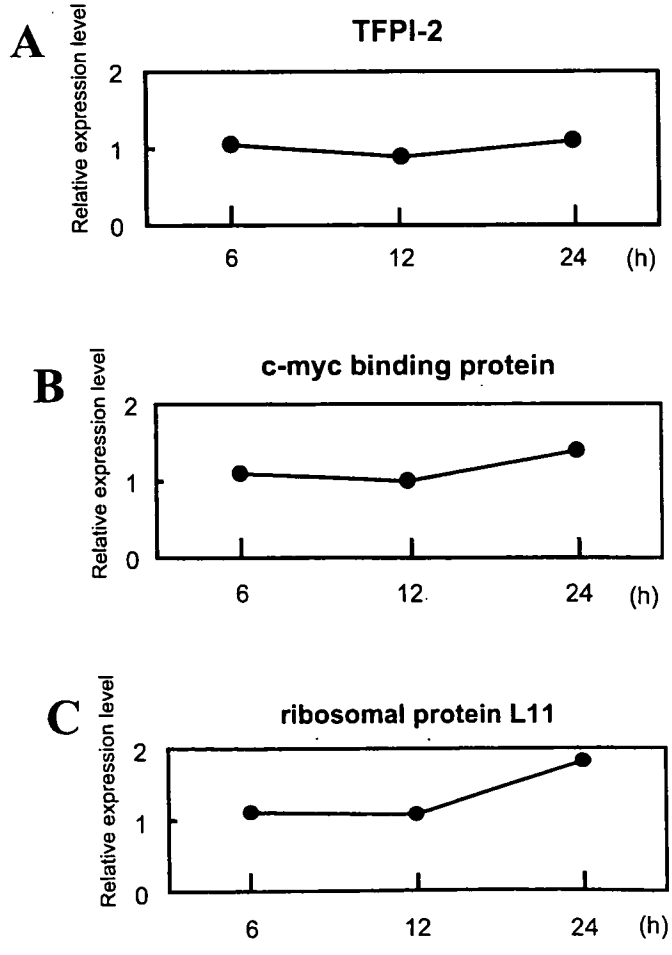

FIGURE 3. Time course of gene expression for TFPI-2 (A), c-*myc* binding protein (B), and ribosomal protein L11 (C) in the cultured human RPE cells after exposure to TFPI-2.

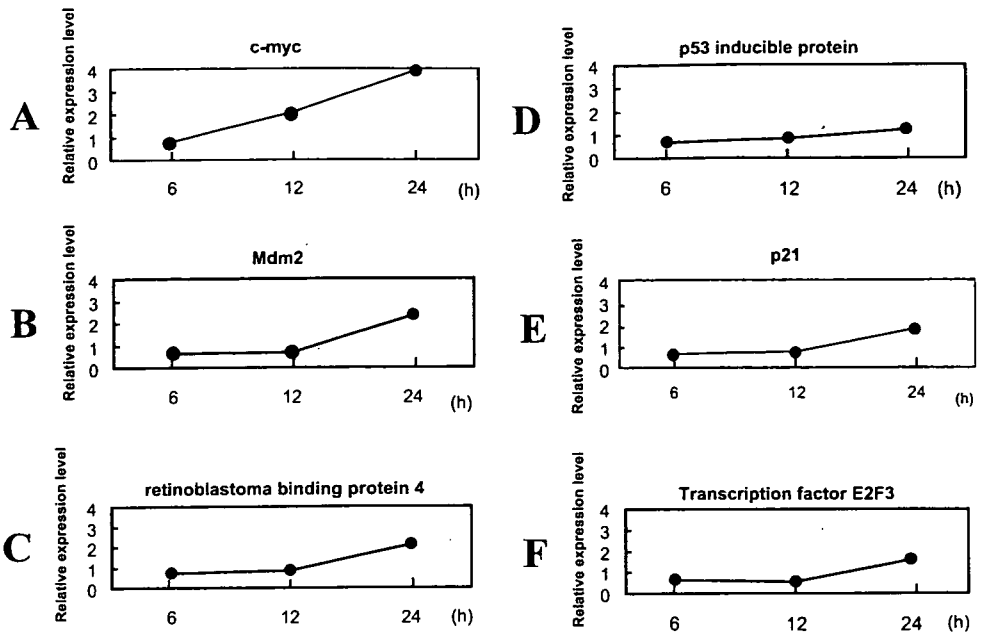

FIGURE 4. Time courses of protein expression patterns for c-*myc* (A), Mdm2 (B), retinoblastoma binding protein 4 (C), p-53 inducible protein (D), p21 (E), and transcription factor E2F3 in the cultured human RPE cells after exposure to TFPI-2.

sion of *Mdm2* might have been involved in the augmented degradation of Rb through the ubiquitin/proteasome-dependent pathway. Recently, Uchida et al.[20] suggested that Mdm2 regulates the function of RB through the ubiquitin-dependent degradation of RB.

The *Rb* gene was the first identified tumor-suppressor gene,[21] and it was recognized as a central component of a signaling pathway that controlled cell proliferation. Specifically, the D-type G_1 cyclins, together with their associated cyclin-dependent kinases (CKDs) Cdk4 and Cdk6, initiated the phosphorylation of Rb and Rb family members, inactivating their capacity to interact with the E2F transcription factors (Fig. 5).[19] This phosphorylation leads to an accumulation of E2F1, E2F2, and E2F3a, which activate the transcription of a large number of genes essential for DNA replication and further cell cycle progression.[22–26] Among the E2F targets are genes encoding a second class of G_1 cyclins, cyclin E, and the associated kinase Cdk2 (Fig. 5).[19] The activation of cyclin E/Cdk2 kinase activity by E2F leads to further phosphorylation and inactivation of Rb, further enhancing E2F activity and increasing the accumulation of cyclin E/Cdk2 (Fig. 5).[19] This feedback loop, which leads to a continual inactivation of *Rb* independent of the action of cyclin D/Cdk4—defined as a junction in cell proliferation response when passaged through the cell cycle—becomes growth factor independent.[25,26] The activity of the G_1 Cdks is negatively regulated by a family of cyclin-dependent kinase inhibitors (CKIs), including $p21^{WAF1}$, $p27^{Kip1}$, and the $p16^{INK4a}$ family.[27] The three upregulated E2Fs associate exclusively with Rb and appear to play a positive role in cell cycle progression.[19]

RPL11 binds the mouse double-minute 2 (Mdm2 is the mouse homologue of Hdm2 in humans) protein with other ribosomal proteins (L23 and L5) to form a complex to inhibit ubiquitin-dependent degradation of p53.[28–30] The RPL11 protein is expressed in ARPE-19 cells.[31] Inhibition of p53 degradation leads to p21 signaling, which participates in the G_1

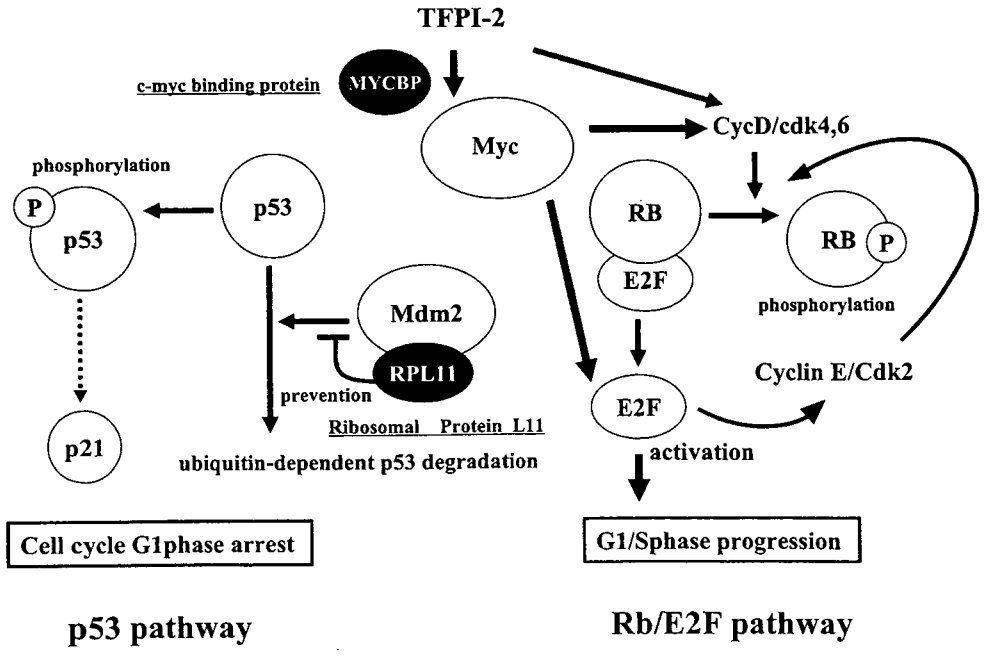

FIGURE 5. Hypothetical network of various genes and proteins associated with the growth-promoting effect of TFPI-2 on the human RPE cells. *Arrows*: stimulatory signals. *Straight* and *dotted lines*: inhibitory effects.

arrest of the cell cycle but also negatively regulates cell proliferation (Fig. 5).[30,32-34] In support of this hypothesis, *p21* transcription was increased by twofold after 24 hours by TFPI-2.

The *p53* gene mediates a major tumor-suppression pathway in mammalian cells and is frequently altered in human tumors.[30] Its function is kept at a low level during normal cell growth and is activated in response to various cellular stresses by acting as a sequence-specific transcription factor.[30] The p53 protein induces cell cycle arrest or apoptosis.[30]

Shinoda et al.[14] reported cell growth proliferation of vascular smooth muscle endothelial cells by a purified mitogenic substance from human umbilical vein endothelial cells, later identified as TFPI-2. These authors showed the rapid activation of mitogen-activated protein kinase (MAPK) by TFPI-2 and the induced activation of proto-oncogene *c-fos* mRNA in smooth muscle cells.[14] They concluded that *c-fos* activation was initiated by MAPK based on MAPK inhibitor PD098059 suppression.

In conclusion, the results of proteomic and transcriptomic analyses suggest that the proliferation of RPE cells induced by TFPI-2 is regulated through the Rb/E2F, p53, and Ras/Raf/MAPK pathways. We and others[3,35] have reported a transcript of TFPI-2 in the mRNA of RPE cells. It is now reasonable to expect that RPE cells are able to self-proliferate by generating TFPI-2. Additional studies are needed to determine whether TFPI-2 can act as such an autocrine factor and can be modified for future treatment of the dry-type age-related macular degeneration and of retinitis pigmentosa.

References

1. Hughes BA, Gallemore RP, Miller SS. Transport mechanisms in the retinal pigment epithelium. In: Marmor MF, Wolfensberger TJ, eds. *The Retinal Pigment Epithelium: Function and Disease*. New York: Oxford University Press; 1998:103-134.
2. Haruta M. Embryonic stem cells: potential source for ocular repair. *Semin Ophthalmol*. 2005;20:17-23.
3. Tanaka Y, Utsumi J, Matsui M, et al. Purification, molecular cloning, and expression of a novel growth-promoting factor for retinal pigment epithelial cells, REF-1/TFPI-2. *Invest Ophthalmol Vis Sci*. 2004;45:245-252.
4. Chand HS, Foster DC, Kisiel W. Structure, function and biology of tissue factor pathway inhibitor-2. *Thromb Haemost*. 2005;94: 1122-1130.
5. Schmidt AE, Chand HS, Cascio D, et al. Crystal structure of Kunitz domain 1 (KD1) of tissue factor pathway inhibitor-2 in complex with trypsin: implications for KD1 specificity of inhibition. *J Biol Chem*. 2005;280:27832-27838.
6. Chand HS, Schmidt AE, Bajaj SP, et al. Structure-function analysis of the reactive site in the first Kunitz-type domain of human tissue factor pathway inhibitor-2. *J Biol Chem*. 2004;279:17500-17507.
7. Sprecher CA, Kisiel W, Mathewes S, et al. Molecular cloning, expression, and partial characterization of a second human tissue-factor-pathway inhibitor. *Proc Natl Acad Sci USA*. 1994;91:3353-3357.
8. Yanamandra N, Kondraganti S, Gondi CS, et al. Recombinant adeno-associated virus (rAAV) expressing TFPI-2 inhibits invasion, angiogenesis and tumor growth in a human glioblastoma cell line. *Int J Cancer*. 2005;115:998-1005.
9. Rollin J, Iochmann S, Blechet C, et al. Expression and methylation status of tissue factor pathway inhibitor-2 gene in non-small-cell lung cancer. *Br J Cancer*. 2005;92:775-783.
10. Konduri SD, Srivenugopal KS, Yanamandra N. Promoter methylation and silencing of the tissue factor pathway inhibitor-2 (TFPI-2), a gene encoding an inhibitor of matrix metalloproteinases in human glioma cells. *Oncogene*. 2003;22:4509-4516.
11. Santin AD, Zhan F, Bignotti E, et al. Gene expression profiles of primary HPV16- and HPV18-infected early stage cervical cancers and normal cervical epithelium: identification of novel candidate molecular markers for cervical cancer diagnosis and therapy. *Virology*. 2005;331:269-291.
12. Sato N, Parker AR, Fukushima N, et al. Epigenetic inactivation of TFPI-2 as a common mechanism associated with growth and invasion of pancreatic ductal adenocarcinoma. *Oncogene*. 2005;24: 850-858.
13. Kast C, Wang M, Whiteway M. The ERK/MAPK pathway regulates the activity of the human tissue factor pathway inhibitor-2 promoter. *J Biol Chem*. 2003;278:6787-6794.
14. Shinoda E, Yui Y, Hattori R, et al. Tissue factor pathway inhibitor-2 is a novel mitogen for vascular smooth muscle cells. *J Biol Chem*. 1999;274:5379-5384.
15. Bahk SC, Lee SH, Jang JU, et al. Identification of crystallin family proteins in vitreous body in rat endotoxin-induced uveitis: involvement of crystallin truncation in uveitis pathogenesis. *Proteomics*. 2006;6:3436-3444.
16. Taira T, Maëda J, Onishi T, et al. AMY-1, a novel C-MYC binding protein that stimulates transcription activity of C-MYC. *Genes Cells*. 1998;3:549-565.
17. West KA, Yan L, Shadrach K, et al. Protein database, human retinal pigment epithelium. *Mol Cell Proteomics*. 2003;2:37-49.
18. Cai H, Del Priore LV. Gene expression profile of cultured adult compared to immortalized human RPE. *Mol Vis*. 2006;12:1-14.
19. Sears RC, Nevins JR. Signaling networks that link cell proliferation and cell fate. *J Biol Chem*. 2002;277:11617-11620.
20. Uchida C, Miwa S, Kitagawa K, et al. Enhanced Mdm2 activity inhibits pRB function via ubiquitin-dependent degradation. *EMBO J*. 2005;24:160-169.
21. Hanahan D, Weinberg RA. The hallmarks of cancer. *Cell*. 2000; 100:57-70.
22. Dyson N. The regulation of E2F by pRB-family proteins. *Genes Dev*. 1998;12:2245-2262.
23. Nevins JR. Toward an understanding of the functional complexity of the E2F and retinoblastoma families. *Cell Growth Differ*. 1998; 9:585-593.
24. Harbour JW, Dean DC. Rb function in cell-cycle regulation and apoptosis. *Nat Cell Biol*. 2000;2:E65-E67.
25. Dou QP, Levin AH, Zhao S, Pardee AB. Cyclin E and cyclin A as candidates for the restriction point protein. *Cancer Res*. 1993;53: 1493-1497.
26. Pardee AB. A restriction point for control of normal animal cell proliferation. *Proc Natl Acad Sci USA*. 1974;71:1286-1290.
27. Sherr CJ, Roberts JM. CDK inhibitors: positive and negative regulators of G1-phase progression. *Genes Dev*. 1999;13:1501-1512.
28. Krystof V, McNae IW, Walkinshaw MD. Antiproliferative activity of olomoucine II, a novel 2,6,9-trisubstituted purine cyclin-dependent kinase inhibitor. *Cell Mol Life Sci*. 2005;62:1763-1771.
29. Dai MS, Lu H. Inhibition of MDM2-mediated p53 ubiquitination and degradation by ribosomal protein L5. *J Biol Chem*. 2004;279: 44475-44482.
30. Zhang Y, Wolf GW, Bhat K, et al. Ribosomal protein L11 negatively regulates oncoprotein MDM2 and mediates a p53-dependent ribosomal-stress checkpoint pathway. *Mol Cell Biol*. 2003;23:8902-8912.
31. Rao KC, Palamalai V, Dunlevy JR, et al. Peptidyl-Lys metalloendopeptidase-catalyzed ^{18}O labeling for comparative proteomics: application to cytokine/lipolysaccharide-treated human retinal pigment epithelium cell line. *Mol Cell Proteomics*. 2005;4:1550-1557.
32. Chao C, Saito S, Kang J. p53 transcriptional activity is essential for p53-dependent apoptosis following DNA damage. *EMBO J*. 2000; 19:4967-4975.
33. Bai F, Matsui T, Ohtani-Fujita N, et al. Promoter activation and following induction of the p21/WAF1 gene by flavone is involved in G1 phase arrest in A549 lung adenocarcinoma cells. *FEBS Lett*. 1998;437:61-64.
34. Nyunoya T, Powers LS, Yarovinsky TO. Hyperoxia induces macrophage cell cycle arrest by adhesion-dependent induction of p21Cip1 and activation of the retinoblastoma protein. *J Biol Chem*. 2003;278:36099-360106.
35. Ortego J, Escribano J, Coca-Prados M. Gene expression of protease and protease inhibitors in the human ciliary epithelium and ODM-2 cells. *Exp Eye Res*. 1997;65:289-299.

Source Book of Models for Biomedical Research

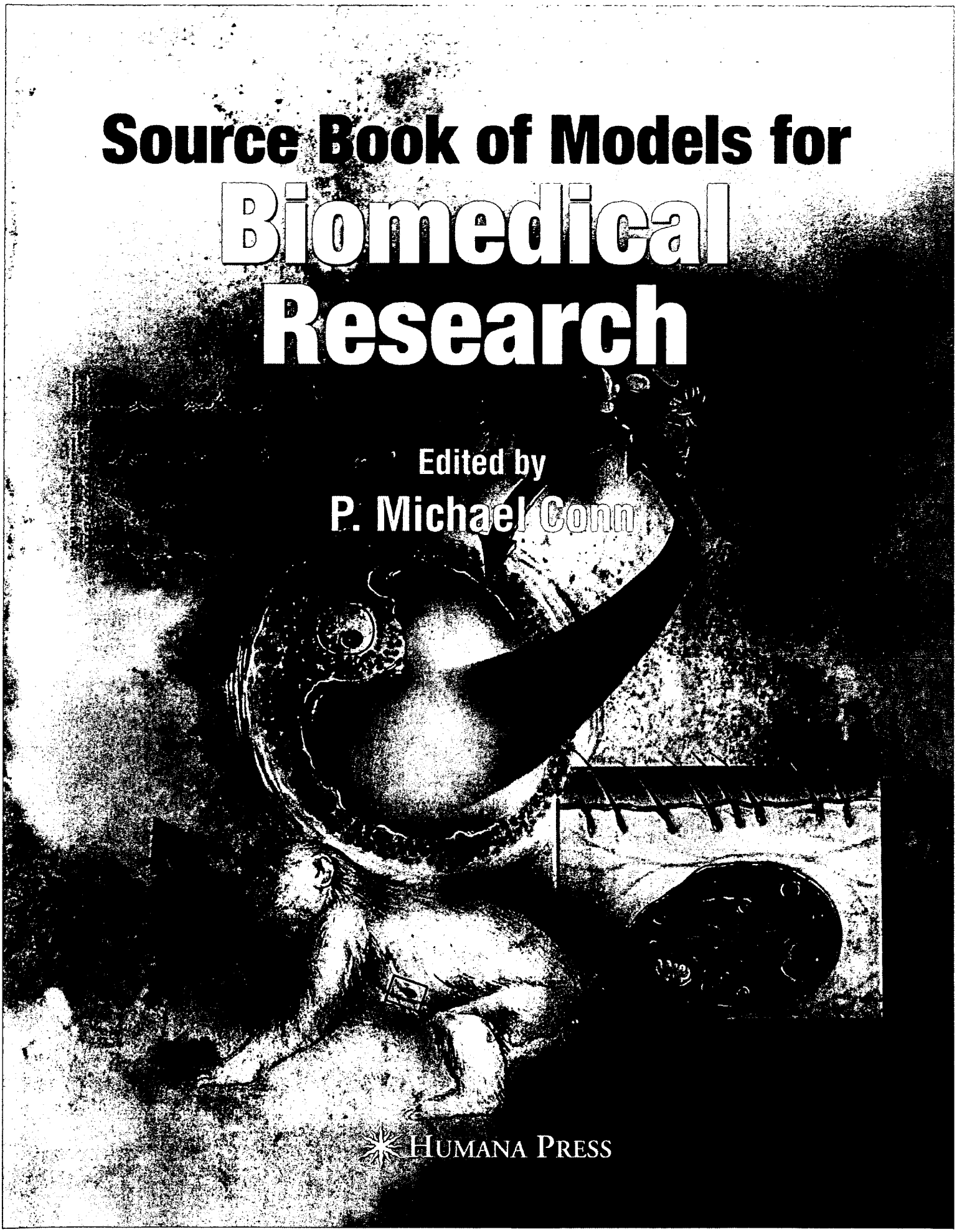

Edited by

P. Michael Conn

HUMANA PRESS

Source Book of Models for Biomedical Research

Chapter 33: Animal Models for Eye Diseases and Therapeutics

Subtitle: Animal models of Age-Related Macula Degeneration and glaucoma

Takeshi Iwata, Ph.D.[1] and Stanislav Tomarev, Ph.D.[2]

[1]National Institute of Sensory Organs, National Hospital Organization Tokyo Medical Center, 2-5-2 Higashigaoka, Meguro-ku, Tokyo 152-8902 Japan.

TEL/FAX: +81-(3)3411-1026

e-mail: iwatatakeshi@kankakuki.go.jp

[2]National Eye Institute, National Institutes of Health, Bldg. 7, Rm. 103, 7 Memorial Drive, MSC 0704, Bethesda, MD 20892-0704 USA.

TEL: (301)496-8524

FAX: (301)496-8760

e-mail: tomarevs@nei.nih.gov

***Key Words**: Vision, Age-related macular degeneration, Retina, Macula, Drusen, Glaucoma, Retinal ganglion cells, Optic nerve*

1. Visual impairment and importance of animal models for eye diseases

It is believed that more than 80% of the information our brain receives comes from the visual system. Dysfunction of the visual system can alter the normal human life style and significantly lower the quality of life. The causes of visual impairments and blindness vary among ethnic groups and the global regions where they live. There are many causes of visual impairments including diabetic complications, infections, and trauma, however the most prevalent causes of visual impairment are cataracts, glaucoma, and age-related macular degeneration (AMD). According to the World Health Organization, there were more than 161 million visually impaired individuals in 2002, and 124 million of this group had low vision and 37 million were blind (http://www.who.int/mediacentre/factsheets/fs282/en/index.html) (Fig. 1).

Cataract, glaucoma, and AMD are responsible for 69% of blindness globally. Although cataracts are the leading cause of blindness worldwide, recent advances in cataract surgery has significantly reduced the visual impairments caused by cataracts especially in developed countries. Glaucoma, an optic neuropathy, is often associated with elevated intraocular pressure and is responsible for blindness in 6.7 million people

across the world. Glaucoma is more common in individuals of African ancestry, and the incidence of glaucoma increases with age.

The most prevalent eye disease for elderly Europeans and Americans is AMD. This degenerative disease progresses from retinal deposits called drusen to neovascularization and retinal hemorrhages resulting in irreversible loss of central vision.

In spite of the high incidence of AMD and glaucoma, a limited amount of information is available on the underlying pathological mechanisms causing these diseases. Obtaining tissues for any disease is often difficult, and even when obtained, they may not be informative because the tissues are usually collected many hours or even days after death. Because experimental studies of AMD and glaucoma are limited in humans, the availability of animal models is very valuable because they can be used to investigate the molecular mechanisms causing these diseases and to test new therapeutic interventions. Animal models, compared to other experimental methods, e.g., cell and organ cultures or postmortem models, allow the study of different pathological factors and therapeutical treatments under in vivo conditions, i.e., with the visual and other systems of the body intact. Appropriate animal models, e.g., monkey,

mouse, zebrafish, also facilitate the identification of new genes involved in the pathology as well as elucidate the genetic relationships between causative and modifier genes. Equally important, specific genes can be altered in these models. Thus, it is possible to induce mutations in animals, and then search for specific phenotypes, e.g., abnormal intraocular pressure (IOP) and retinal ganglion cell degeneration. Subsequently, the affected genes can be identified by standard genetic procedures.

Many animal models of AMD and glaucoma have been developed in different mammalian and non-mammalian species. None of these models is a perfect reproduction of the human disease, and when choosing the animal model for research, the investigator should evaluate the following: 1) similarity of the visual system of the model to that of humans especially the eye; 2) similarity of the time course of pathological changes in the model and in human eyes; 3) ability to perform genetic manipulations; 4) training required to produce affected animals; 5) size of the eye; 6) availability and difficulties in the methods of analysis; 7) availability of animals; and 8) cost.

2. Age-related macular degeneration (AMD)

2.1. Introduction of AMD

The retina is composed of nine layers of neural and glial cells that are arranged concentrically at the posterior pole of the eye. Incoming light is focused on the central area of the retina called the fovea which is located in the center of the macular area (Fig. 2). In humans, the size of the macula is approximately 6 mm in diameter (Fig.3). The outer (posterior) surface of the retina is covered by a monolayer of retinal pigment epithelial (RPE) cells which forms a diffusion barrier between the neural retina and the choroidal blood supply. The RPE regulates the transport of proteins to the retina, and controls the hydration and ionic composition of the subretinal space. The physiological condition of the RPE is closely associated with the pathogenesis of AMD.

AMD is a blinding disorder characterized by a marked decrease in central vision associated with RPE atrophy with or without choroidal neovascularization (CNV). Many factors including genetic, behavioral, and environmental, are involved in this disease. AMD is characterized by the degeneration of cone photoreceptors in the foveal region of the retina resulting in a decrease of central visual acuity. The progressive impairment of

the retinal pigment epithelial (RPE) cells, and damage to Bruch's membrane and choriocapillaris results in retinal atrophy and photoreceptor dysfunction. In some cases, CNV develops, and the new vessels penetrate Bruch's membrane and pass into the subretinal space.

Two types of AMD are recognized; the non-neovascular type is called the dry-type AMD and includes more than 80% of the cases, and the neovascular type is called the wet-type AMD which is progressive with a higher probability of blindness. The prevalence of AMD differs considerably among the different ethnic groups, but the incidence increases with age in all groups. A lower prevalence of AMD has been reported in individuals of African ancestry than of Anglo-Saxon ancestry. Other risk factors for AMD are cigarette smoking, obesity, hypertension, and atherosclerosis.

2.2. Epidemiology and genetics of AMD

Extensive epidemiological studies have shown a genetic component for AMD. Thus, twin studies have shown a higher concordance for AMD in monozygotic twins than in dizygotic twins (1-3). In addition, first degree relatives of individuals with AMD

have a 2 to 4 fold higher incidence of AMD over individuals without a family history of AMD. Genetic segregation studies have also shown a genetic effect that accounts for approximately 60% of AMD with a single major gene accounting for about 55% of the risk of developing AMD. Overall, the data have suggested that the etiology of AMD has a significant genetic component. Only a small proportion of the families with AMD show Mendelian inheritance, and the majority of the individuals inherit AMD in a complex multi-gene pattern.

There have been a number of attempts to identify the genes which cause AMD. With the help of the haplotype marker project (HapMap Project), genome wide scanning has identified at least 13 loci linked to AMD on different chromosomes (4-6).

Recently, a polymorphism of complement factor H gene (*Y402H*) was shown to be associated with an increased risk for AMD (7-10). These results were confirmed in many of the countries with large Caucasian populations but not in Japan (11,12). This gene is located on chromosome 1q25-31 where one of the candidate loci was identified by linkage studies. Another recent study reported that a haplotype association of tandemly located complement 2 and factor B was protective for AMD (13).

2.3. Pathology and biochemistry of AMD

The early stage of the dry type AMD is characterized by a thickening of Bruch's membrane, aggregation of pigment granules, and increasing numbers of drusen. The thickening of Bruch's membrane obstructs its function as a 'barrier' between the choroid and the RPE that protects the neural retina from the choriocapillary. Drusen are small yellowish-white deposits that are composed of lipids, proteins, glycoproteins, and glycosaminoglycans. They accumulate in the extracellular space and the inner aspects of Bruch's membrane (Fig. 3). Drusen are not directly associated with visual loss but represent a risk factor for both the dry-type and wet-type AMD. The classification of hard and soft drusen is based on their size, shape, and color; hard drusen are yellowish with diameters <50 μm and are found in eyes that are less likely to progress to advanced stages of the disease, while soft drusen are darker yellow and larger in size, and are found in eyes more likely to progress to more advanced stages of AMD. A small percentage of dry-type AMD patients progress to the late stage of the wet-type AMD that is characterized by geographic atrophy or detachment of RPE and the

development of CNV in the macular region. The presence of a CNV is the factor that most damages the neural retina because the newly developed vessels grow from the choriocapillaris through Bruch's membrane and extend laterally through the RPE cell layer (classic CNV) or extend between the inner Bruch's membrane and RPE (occult CNV). In advanced stages of AMD, the CNV and fluid leaked into the subretinal or intraretinal regions leads to cell death and retinal detachment.

Recent analyses of the progression of drusen have provided important clues that help understand the molecular pathology of AMD. Using both immunohistochemistry and proteomic techniques, the materials in drusen were found to be composed of molecules that mediate inflammatory and immune processes (14, 15). These molecules include components of the complement pathway and modulators of complement activation, viz., vitronectin, clusterin, membrane cofactor protein, and complement receptor-1. In addition, molecules triggering inflammation, viz., amyloid P component, a1-antitrypsin, and apolipoprotein E, were identified in drusen. Cellular debris from macrophages, RPE cells, and choroidal dendritic cells has also been identified in drusen. On the other hand, crystallins, EEFMP1, and amyloid-beta have been found at